ANTIPROTON-DEUTERON LOW ENERGY CROSS-SECTION

R. Bizzarri, P. Guidoni, F. Marcelja* and F. Marzano

Istituto di Fisica dell'Università - Roma
Istituto Nazionale di Fisica Nucleare - Sezione di Roma

E. Castelli and M. Sessa

Istituto di Fisica dell'Università - Trieste
Istituto Nazionale di Fisica Nucleare - Sezione di Trieste

* Present address: Stanford Linear Accelerator Center,
Stanford, California, U.S.A.

ABSTRACT

About 45.000 interactions of antiprotons of kinetic energy between 57 and 170 MeV have been measured in a deuterium bubble chamber. Total and annihilation cross-sections have been determined at 9 values of the antiproton energy together with the differential cross-section $d\sigma/dt$ for scattering events. In spite of the peculiar behaviour of the deuteron target at these low energies a reliable measure of the antiproton-neutron annihilation cross section has been obtained.

1. - INTRODUCTION

In this paper are presented the results of a high statistics study of the general features of the interactions of antiprotons in deuterium in the laboratory momentum range 300 to 600 MeV/c. This is part of a systematic study of the antiproton nucleon interaction at these energies, the results obtained in hydrogen having already been published ([1,2,3]). This further investigation is an attempt to extract informations on the $\bar{p}n$ interaction in order to detect the influence of the I-spin on the $\bar{N}N$ interaction, the $\bar{p}n$ system being pure I=1 while the $\bar{p}p$ is a mixture of I=1 and I=0.

The interest in the study of the $\bar{N}N$ interactions in this energy range can be attributed to two main motives. First, the attempt to understand the low energy $\bar{p}p$ interaction. Ball and Chew ([4]) have first shown that the real part of the $\bar{p}p$ potential can be obtained from the pp potential by changing the sign of the terms corresponding to odd G-parity exchanges. No theoretical predictions however exist for the interaction responsible for annihilation which has to be added on purely phenomenological grounds. This can be done either by imposing a boundary condition (incoming wave only) at a given $\bar{p}p$ separation or by adding a suitable imaginary potential. Various calculations have been done along these lines, using more refined pp potentials and taking advantage of the improved experimental data to better fit the annihilation interaction ([5]). The most recent and most successfull in reproducing the $\bar{p}p$ cross sections is the one by Bryan and Phillips ([6]) which makes use of the Bryan and Scott ([7]) pp potential and represents annihilation by means of an imaginary potential of the Saxon-Wood type, fitted to the experimental data. In this and most of the previous calculations the annihilation is assumed to have no spin or I-spin dependence. The real part of the potential however gives rise to a difference in the predicted $\bar{p}p$ and $\bar{p}n$ annihilation cross sections which is interesting to check experimentally.

A second motive of interest comes from the possible existence of a meson of mass 1920-1950 MeV/c^2 which could possibly be formed in $\bar{N}N$ interaction (S-meson). Although the detection of such a meson might be easier via the study of particular final states ([8]), the knowledge of the energy behaviour of the total cross sections is a necessary starting point for this search. The relevance of part of the data presented in this work on the problem of S-meson formation has been discussed in a previous paper ([9]).

The fact that the $\bar{p}n$ interaction has to be studied on deuteron targets poses problems of interpretation since the usual Glauber theory of deuteron interaction has been constructed for high incident energies and its application at these low energies might be questionable. On the other hand the present data give informations which might be useful for a better understanding of the behaviour at low energy of the deuteron target. No attempt in this direction is however made in this article.

In the next section our experimental procedure will be discussed. In sect. 3 we give the deuteron cross sections. In sect. 4 the spectrum of the "spectator" protons and in sect. 5 the ratio of $\bar{p}p$ to $\bar{p}n$ annihilation cross sections are discussed. In sect. 6, after comparing present results with those obtained in H_2, an estimate of the $\bar{p}n$ annihilation cross section is given. The scattering is discussed in sect. 7.

The data presented in this work are in general agreement with the previous data. of comparable statistical accuracy, obtained by Burrows et al. [10] on the $\bar{p}d$ cross sections in this same momentum range.

2. - EXPERIMENTAL PROCEDURE

i) Beam and exposure. The film was obtained by exposing the 81 cm Saclay deuterium-filled bubble chamber to a separated antiproton beam from the CERN P.S. Three exposures (in the following called I, II, III) have been made at beam momenta of 620, 670 and 715 MeV/c respectively (see tab. I). A Cu moderator of 4.5 g/cm^2 was placed in front of the beam entrance window of the bubble chamber. A fourth exposure (exposure 0) with a beam momentum of 620 MeV/c and the moderator thickness increased to 13.5 g/cm^2 of Cu was also made. The antiprotons then stopped about in the center of the chamber and this last exposure was used for beam calibration purposes.

ii) Scanning. The film was scanned for all the $\bar{p}$ interactions. The very small meson contamination in the beam was readily distinguishable because of the smaller ionization and the larger radius of curvature (due to the smaller energy losses in the absorber). Since the beam energy is always below the threshold for pion production the interactions were classified into two groups:

a) scatterings (with or without deuteron breakup): the antiproton reemerges from the interaction and a recoil (deuteron or proton) is sometimes visible.

b) annihilations: the antiproton disappears and an even (including zero) or odd number of charged mesons is produced together with a neutron or a proton respectively. In 58% of cases the proton is too slow to give rise to a visible track.

Because of the low velocity of the incident antiprotons these two types of reactions are readily distinguishable by visual inspection. The scanning efficiency for the annihilation events was found by double scanning on a fraction of the film to be 99%. For the scattering events it depends on the scattering angle as it will be discussed in sect. 3.

In the 0-prong events are included also the final states $nn\bar{n}$ which can not be distinguished from the annihilations into neutral mesons.

iii) Measurements. The events have been measured on image plane digitizers with a measuring precision of ~ 0.1 mm in the bubble chamber space. All the tracks of the scattering events have been measured. For the annihilation events only the interaction point and the incident antiproton track have been measured. Furthermore even pronged events have been inspected to detect the possible presence of a proton. All the protons stopping in the chamber have been measured. In half of the film all the tracks which by visual ionization estimate appeared to be protons have been measured even if they were leaving the chamber.

To determine the total track length scanned the non-interacting tracks have been measured every tenth picture.

Both the events and the non-interacting tracks were reconstructed in space by the CERN program THRESH. The events which failed geometrical reconstruction were re-measured twice. Events still failing after the third measurement were only about 1%.

iv) Selection of the events. A fiducial volume of interaction has been defined by an entrance and an exit fiducial plane. The position of these planes is shown in Fig. 1. The entrance fiducial plane is choosen in such a way as to ensure at least 6 cm of illuminated $\bar{p}$ track before the interaction. The exit fiducial plane is choosen in such a way as to guarantee a good measurability of the interaction products and it is slightly inclined in the lowest energy exposure due to the larger bending of the beam tracks. The primary tracks were also requested to cross the entrance fiducial plane inside a beam area about 9×13 cm^2 and within a given cone ($\sim$0.05 steradiants) about the average beam direction. These cuts have been choosen in such a way as to guarantee that the antiproton tracks enter the chamber by going through the beam entrance window and that they stay well inside the illuminated region of the chamber up to the exit fiducial plane. In this way antiprotons undergoing a nuclear scattering in the absorber are also eliminated. Furthermore the primary tracks have been extrapolated back to the plane AA (see Fig. 1) where the copper moderator was placed in order to check that they had crossed this plane going through a constant thickness of Cu without hitting the mechanical supports of the moderator.

These cuts eliminated a percentage of events varying from 44% in exposure I to 25% in exposure III (see Tab. I). The same cuts were applied to the non-interacting tracks.

v) Energy scale and resolution. The average momentum of the $\bar{p}$ at the entrance of the fiducial region is determined from radius of curvature measurements on the non-interacting tracks surviving the above described selections. The momentum distribution for the tracks from exposure II is shown as an example in Fig. 2. It is very nearly gaussian, with no detectable tails, and allows a measurement of the average beam momentum to an accuracy limited by the systematic errors in the radius of curvature measurements, estimated to be less than 1%.

The observed r.m.s. spread of the above distribution is $\pm$12 MeV/c and it is mostly due to multiple scattering, which contributes at this energy about $\pm$ 10 MeV/c.

The true momentum spread of the beam can instead be determined from the track length distribution of the annihilating antiprotons from exposure 0, shown in Fig. 3. The average range is 22 cm with an r.m.s. spread of about $\pm$ 4 cm of liquid deuterium corresponding to $\Delta p/p$ = 0.8% at the bending magnet (620 MeV/c). The same $\Delta p/p$ can be assumed for the beam settings of the II and III exposure and the corresponding values of the uncertainty in the residual range are $\pm$5 and $\pm$ 6 cm of liquid deuterium.

Since the momentum spread of the beam is smaller than the multiple scattering error on individual radius of curvature measurements, we shall attribute to each interacting $\bar{p}$ the average momentum as deduced from the beam value at the entrance and its path length in the chamber.

The density of the liquid deuterium was determined by muon range measurements on 180 π-μ decays to be 0.137 ± 0.001. The average value of the range of the stopping antiprotons in exposure 0 computed from the measured curvature using the above density agrees with the measured value.

3. - CROSS-SECTIONS

Before computing cross-sections the measured number of events has been corrected for various losses. The annihilation events had a 1% correction for scanning losses and a further correction of 2.5% because of losses of events in the geometrical reconstruction program (1%), losses in bookeeping (0.5%) and events not measurable for various reasons (1%).

The scattering events had this same 2.5% loss. The scanning efficiency for those events depends strongly on the scattering angle. To avoid large and uncertain efficiency corrections we have retained only events with a $\bar{p}$ scattering angle larger than 7° in space. The scanning efficiency for these events was found by double scanning to be 98%.

Two further corrections have then be applied to obtain the true number of scattering events:

i) there is a loss of events when the plane containing the incident and scattered $\bar{p}$ tracks makes an angle near 90° with the chamber window. The azimuthal distribution of the scattered antiproton about the incident track (which should be isotropic for unbiased events) shows that this loss amounts to about 5% of the events.

ii) the number of nuclear scatterings at angles smaller than 7° has been estimated by extrapolating to t=0 the differential cross-section $\frac{d\sigma}{dt}$ (see sect. 7). Due to the rapid decrease of $\frac{d\sigma}{dt}$ with t, this correction is quite large varying from 10% to 18% with increasing energy. This introduces an uncertainty of about 2% in the scattering cross-section.

The events have then been grouped according to the $\bar{p}$ range in deuterium after the fiducial entrance plane. Intervals of 16 cm of liquid deuterium have been used giving a total of nine (three for each exposure). The number of events in each interval has then been used to compute the cross section:

$$\sigma = \frac{n}{N\,L}$$

n = number of events corrected for the various losses
N = number of atoms/cm^3 in the chamber liquid
L = total length of track crossing the interval

In this way we have obtained the total scattering and inelastic (annihilation and charge exchange) cross sections σ_s and σ_i as given in Table II and in Fig. 4, where the results of ref. ([10]) are also shown for comparison.

The average energy for each cross section point has been given as the average beam energy at the center of the interval. The energy distribution inside each interval is obtained by folding the gaussian beam distribution with the finite size of the range interval. Three examples are shown on the abscissa axis of Fig. 4. In Table II the half width at half height of these energy interval are given. About 80% of the events are within these limits.

4. - ANNIHILATIONS WITH A PROTON OR A NEUTRON IN THE FINAL STATE AND BEHAVIOUR OF THE SPECTATOR PROTON

To obtain informations on the antiproton - neutron annihilation cross-sections we must identify the events where a proton is emitted together with an odd number of charged pions. Certainly all the odd pronged events belong to this cathegory, the emitted proton being in this case too slow to give a visible track. As for the even pronged events, they can certainly be attributed to $\bar{p}n$ annihilations if a positive track stops without decay in the chamber. The even pronged annihilations without a a stopping proton have been scanned in one half of the film and whenever a track was found which by ionization and curvature appeared to be a proton, it was measured as such.

The resulting proton spectrum for momenta above 120 MeV/c is shown in Fig. 5.a and compared with the expected distribution from the Hamada - Johnston ([11]) wave function normalized to the number of events below 120 MeV/c. It is apparent an excess of high momentum protons, this effect being of the same magnitude as observed in other annihilation experiments ([12-17]). With the same cut at $P > 120$ MeV/c, in Fig. 5.b,c are also shown the distributions of the components of the proton momentum transverse (P_t) and parallel (P_ℓ) to the beam direction. Both show the same excess of energetic protons. The distribution of P_ℓ shows also a preference of the fast protons for the forward hemisphere.

From this data the percentage of protons leaving the chamber is (17±2)%. The error is not statistical but rather an estimate of the possible losses or misidentifications of energetic protons. It corresponds to a 100% uncertainty on the number of protons with momentum bigger than 700 MeV/c (corresponding to an ionization of 3 times the minimum). The number of protons leaving the chamber has also been estimated by a Montecarlo assuming the proton momentum spectrum to be the same as measured at rest in a large bubble chamber ([18]), the result being then 17.5%, in agreement with the direct estimate.

With these corrections we can compute the annihilation cross-sections with the production of an odd ($\sigma_{i,n}$) or even ($\sigma_{i,p}$) number of charged mesons as given in Table II. The cross sections for annihilation into charged prongs ($\sigma_{i,2+4+6}$) and for zero-prong events ($\sigma_{i,o}$) have been given separately since to this last cross-section there is an important contribution of the charge exchange reaction which will be discussed in the section 6. The cross-sections for annihilations into different number of charged mesons (1 to 6) are given in Table III. In the last row of tables II and III the relative frequencies of different annihilation channels for antiprotons at rest are also given. These data are obtained from exposure 0 considering the $\bar{p}$ tracks longer than 16 cm (see Fig. 3).

The ratios of the in fligth topological cross-sections do not show significant variations in this energy interval and (except for the zero-prong events) are not different from those obtained at rest. The frequency ratios of the even pronged events agree also with those obtained from $\bar{p}p$ annihilations.

5. - RATIO OF $\bar{p}p$ TO $\bar{p}n$ ANNIHILATION CROSS-SECTIONS

The data obtained in the previous section could be interpreted in the framework of the impulse model as representative of $\bar{p}n$ or $\bar{p}p$ annihilations according to the presence in the final state of a "spectator" proton or neutron respectively. Some consideration, however, has to be given to the fact that annihilation occurs on a deuteron.

The first effect to consider is the possibility of scattering (including charge exchange) of the antinucleon before annihilation. The $\bar{p}d$ system is a state of definite I-spin, $I = 1/2$, $I_3 = -1/2$. With the sole assumption that the annihilation reaction produces a meson cloud of I-spin not greater then 1 plus a nucleon, charge independence implies that the cross-section for annihilation with a proton in the final state is proportional to $|A_1|^2$ and with a neutron to $1/2(|A_1|^2+|A_0|^2)$ independent of the possible complexities of the initial state interaction ($A_{1,0}$ indicates the annihilation amplitude to produce a meson cloud of I-spin 1 or 0).

The final state interaction could, in principle, alter the neutron-proton ratio of the outgoing nucleons via charge exchange rescattering of the pions produced in the annihilation on the spectator nucleon according to the reactions

$$\pi^+ n \leftrightarrows \pi^0 p$$
$$\pi^0 n \leftrightarrows \pi^- p$$

which can proceed in both ways, to change a neutron into proton or viceversa.

Since the average charged annihilation multiplicities do not change in going from rest to our energies, the existing data for $\bar{p}p$ and $\bar{p}n$ annihilations at rest([13, 15,19,20]) have been used to estimate the average number <n> of π which can give the charge exchange rescattering. These numbers are summarized in Table IV. The last column of this table takes into account the fact that 45% of $\bar{p}d$ annihilations are on neutrons and 55% on protons. These data show an almost complete compensation between charge exchange reactions transforming p into n and viceversa: the effective number of pions to transform a neutron into a proton is only ~2.0-1.8 ≃ 0.2 per annihilation, with an uncertainty ~100%. Furthermore the charge exchange cross section averaged over the pion spectrum is ~30 mb i.e. quite smaller that $4\pi/\langle r^{-2}\rangle \simeq 450$ mb (r being the two nucleon separation in the deuteron) and therefore this rescattering effect is not expected to be significant within the accuracy of the data.

It can then be concluded that the simple ratio of the events with an outgoing proton to those with a neutron is indeed a good measure of the ratio of $\bar{p}n$ to $\bar{p}p$ annihilation cross-sections.

This information is summarized in the last three columns of Table III. The ratio of the $\bar{p}n$ to $\bar{p}p$ inelastic cross-sections has been computed including (R') or excluding (R") from this last cross-section the contribution of the zero prong events. Since these events contain both charge-exchanges and annihilations into neutral mesons the true ratio R of the annihilation cross-sections is in between R' and R". The best estimate of R is given in the last column of Table III and it is obtained assuming the annihilation into neutral mesons to represent 4.7% of the annihilation into charged prongs (see next section). The value of R is about 0.8 (corresponding to $|A_0|^2 \sim 1.5\, |A_1|^2$) and does not show significant variations with energy. At rest we have R = 0.81±0.03.

The measured R is lower than the value 0.9 predicted by the calculations of Bryan and Phillips [6] for the static OBE (one boson exchange) potential (the non static case predicts slightly larger values). This discrepancy does not imply a failure of the model since the difference in the predicted $\bar{p}p$ and $\bar{p}n$ annihilation cross-sections is due to the real part of the potential and it depends largely on the OBE terms of shorter range than the one pion exchange which are certainly less known. More important, the effective role of these terms is influenced by the assumed shape of the tail of the imaginary potential and the discrepancy might probably be cured by small adjustements of this phenomenological ingredient.

6. - COMPARISON WITH THE RESULTS IN HYDROGEN AND THE $\bar{p}n$ ANNIHILATION CROSS SECTION

In Fig. 6 the cross-sections for $\bar{p}p$ annihilation into charged prongs and for 0-prong events as obtained from this experiment are compared with the results obtained in hydrogen [1]. It is apparent that the annihilation cross-section does not change in going from H_2 to D_2 while there is a significant reduction of the zero prong cross-section. This fact deserves some discussion.

0- prong. From the observation of $\bar{n}$ stars Bizzarri et al. [3] have estimated the charge exchange to represent 75% of σ_0 in $\bar{p}p$ interactions in this same energy range. This estimate required a guess of the $\bar{n}p$ annihilation cross section which was based on very preliminary results on the charge conjugate reaction $\bar{p}n$ from this experiment.

The present result confirms that guess and increases our confidence on the estimate of ref. ([3]). We can therefore safely assume that in $\bar{p}p$ interactions the annihilation into neutrals represents ~25% of the 0-prong cross-section i.e. ~4.7% of the annihilation cross-section into charged prongs.

The reduction in the 0-prong cross-section can therefore be attributed to the charge exchange reaction $\bar{p}d \to nn\bar{n}$ and accounted for by the Pauli principle, due to the small average momentum transfered to the neutron. The importance of this effect has been estimated by assuming the charge exchange to be dominated by the non spin-flip amplitude and multiplying the charge exchange angular distributions of ref. ([3]) by the appropriate deuteron weight factors ([21]). The resulting reduction in the cross-section is 5.2±0.8 mb at 100 MeV and 3.1±0.6 mb at 150 MeV in agreement with the observed effect.

Annihilation cross-section. The fact that the $\bar{p}p$ annihilation cross-section as measured in deuterium is not different from the cross-section measured in hydrogen is somehow surprising. In the framework of the Glauber theory of high energy interactions in deuterium ([22]) one would have expected a cross-section defect of 15 ÷ 20 mb on the $\bar{p}p$ annihilation cross-section. A fit of the experimental data with a smooth curve (of the type $\sigma \propto 1/p$) indicates on the contrary an average defect of ~(1 ÷ 2) mb (with the exception perhaps of the lowest energy point).

The failure of the Glauber theory at these low energies migth be not surprising. But, even in the absence of a satisfactory treatment of the multiple scattering corrections, we can make use of the fact, discussed in the previous section, that they should not alter the ratio R of $\bar{p}n$ to $\bar{p}p$ annihilation corss-sections. The absence of a cross-section defect in $\bar{p}p$ annihilation can therefore be taken as a strong indication that the measured $\sigma_{i,n}$ is a good estimate of the cross-section on free neutrons. This cross-section is shown in Fig. 7 compared with the prediction of Bryan and Phillips ([6]). The theoretical prediction is somewhat higher than the experimental points as discussed in the previous section.

The neutron target, being bound, is not stationary and the measured cross-sections are averaged over the target momentum in the deuteron:

$$\langle\sigma\rangle = \int d^3q \, |\psi(q)|^2 \, \frac{v(\bar{p},\bar{q})}{v(\bar{p},o)} \, \sigma(\bar{p},\bar{q})$$

where $v(\bar{p},\bar{q})$ is the relative velocity of an incident particle of momentum $\bar{p}$ on a nucleon of momentum $\bar{q}$, $\sigma(\bar{p},\bar{q})$ is the cross-section in this configuration and ψ (q) is the deuteron wave function in momentum space. Since the cross-sections vary nearly as $1/v$, this energy dependence cancels with the flux factor and one has simply $\langle\sigma\rangle = \sigma(p)$.

If the annihilation cross-section however had rapid variations with energy, the deuteron structure would cause a loss of energy resolution, which can be estimated to be

$$\Delta E^2_{c.m.s.} \simeq \sqrt{\langle(\bar{p}\cdot\bar{q})^2\rangle} = \frac{1}{\sqrt{3}}\, p \sqrt{\langle q^2\rangle}$$

The value of $\sqrt{\langle q^2\rangle}$ on the whole deuteron wave function is ~150 MeV/c, thus giving $\Delta E^2_{c.m.s.} \simeq 0.43$ GeV^2 at p = 0.5 GeV/c corresponding to a r.m.s. uncertainty on the incident momentum $\Delta p \simeq 60$ MeV/c. For the $\bar{p}n$ annihilation cross-section a good improvement can be obtained selecting those events with an unseen spectator proton. This reduces $\sqrt{\langle q^2\rangle}$ to ~50 MeV/c giving, always at p = 500 MeV/c, $\Delta E^2_{c.m.s.} \simeq 0.15$ GeV^2 and $\Delta p \simeq 20$ MeV/c. The cross-section obtained from these events is shown in the last column of Table II. These data have been used in ref. (9) to discuss the possible resonance formation at these energies.

A qualitatively correct phenomenological description of the $\bar{N}N$ annihilation can be obtained by imposing a boundary condition of only incoming waves at the surface of a sphere of radius R_N. This predicts an annihilation cross section $\sigma_n = \pi(R_n+\lambda)^2$ which fits the data with $R_n = .77\pm.01$ fm. For comparison the $\bar{p}p$ inelastic cross-section (including 0-prong) requires $R_p = 1.05\pm.01$ fm.

7. - SCATTERING

13600 scattering events are present in our sample, 46% of them had a measurable recoil track (proton or deuteron). The events have been fitted with the CERN kinematic program GRIND to the two hypotheses of elastic ($\bar{p}d\to\bar{p}d$) and inelastic ($\bar{p}d\to\bar{p}pn$) scattering. Due to the small average momentum transfer in the reaction, for most of the events the fit is unable to discriminate the two hypotheses: 26% of the events fit only the $\bar{p}pn$ and 7% only the $\bar{p}d$ final states, while the remaining 67% fit both hypotheses.

The angular distribution of the measurable recoils with respect to the $\bar{p}$ beam is shown in Fig. 8. The qualitative features of this distribution are those expected for a scattering on the positive particle: the kinematical limit is at 90° in the laboratory, recoils near 90° have too low an energy to give a visible track and the forward region is very little populated due to the decrease of the cross section with momentum transfer. However one would have expected also an isotropic component in this distribution due to the spectator protons from the $\bar{p}n$ scattering. The absence of this isotropic component indicates that most of the events are either elastic or multiple scatterings involving both nucleons. This is to be expected because the average momentum transfered in $\bar{N}N$ scattering is of ~150 MeV/c, comparable to the average momentum in the deuteron wave function.

A separation of the events into scattering on neutrons and on protons is therefore impossible. The only physically significant quantity which can be measured for each event is the four momentum transfer t of the antiproton whose numerical value for the kinematically ambiguous events is very nearly the same for the elastic or inelastic fits. The $d\sigma/dt$ thus obtained are shown in Table V and Fig. 9, together with the optical points obtained from σ_t. These cross-sections decrease with -t faster than the corresponding $\bar{p}p$ cross-sections.

For $-t \leq 0.025\ (GeV/c)^2$ the cross-sections behave very nearly like $e^{-b|t|}$. A fit with this formula has been performed, taking into account the optical point. The results are shown in Table VI together with the values of the corresponding diffraction radius $R = 2\sqrt{b}$. An antishrinkage of the diffraction peak is observed in analogy with the results on $\bar{p}p$ scattering ([2]).

Assuming at low momentum transfers the cross-section to be mostly elastic, one could expect a slope $b \simeq \frac{1}{2} b_d + b_N$, where b_d is the slope of the deuteron form factor ($b_d \simeq 2.5\ fm^2 = 62\ (GeV/c)^{-2}$) and b_N the slope of the elastic $\bar{p}N$ scattering which can be taken as the average of the two slopes b_p and b_n on proton and neutron respectively. As for the elastic antiproton-proton scattering it is known ([2]) that $b_p = \frac{1}{4}(R_p + \lambda\!\!\!^-)^2$ whith $R_p \simeq 1.03$ fm. Assuming similarly $b_n = \frac{1}{4}(R_n + \lambda\!\!\!^-)^2$, with $R_n = 0.77$ fm, we obtain values of b quite near to the experimental ones. Because of the neglect of the multiple scattering and deuteron break-up contributions this agreement is not very significant. A better understanding of the theory of interaction on deuterons at these low energies would be necessary to extract from the data informations on the slope of the antiproton-neutron scattering.

8. - CONCLUSION

This experiment clearly shows the difficulties of interpretation of deuteron cross-sections in terms of single nucleon amplitudes at low energies, the most striking effect being the very near equality of the $\bar{p}p$ annihilation cross-sections measured in deuterium and in hydrogen. This lack of shadow is most surprising since the $\bar{N}N$ scattering amplitude is strongly peaked in the forward direction, thus producing large interference effects between the two nucleons. In fact the scattering data show a cospicuous forward peak of diffractive character whose slope decreases with increasing energy. Furthermore the angular distribution of the positive particles shows an almost complete absence of "spectator" protons, thus indicating the general partecipation of both target nucleons to the interaction. A complete analysis of the data and the extraction of informations on the $\bar{p}n$ scattering cross-section are therefore hindered by the lack of an adequate theory.

In spite of these difficulties with the deuteron structure, our data allow a reliable measure of the $\bar{p}n$ annihilation cross-section. This cross-section has a smooth decrease with energy being over all our energy range equal to $\sim$80% of the $\bar{p}p$ annihilation cross-section.

It is a pleasure for us to acknowledge the efficient and patient work of our scanning and measuring staff. Mr. F. Beccari and Mr. V. Valente have contributed most of the necessary programming work. We are grateful to Dr. G. Viola and Dr. A. Or landini for their contribution to the early stages of this work and to Prof. G. Albe ri and Dr. L.A. Kondratyuk for stimulating discussions.

REFERENCES

(1) U. Amaldi jr., B. Conforto, G. Fidecaro, H. Steiner, G. Baroni, R. Bizzarri, P. Guidoni, V. Rossi, G. Brautti, E. Castelli, M. Ceschia, L. Chersovani and M.Sessa: Nuovo Cimento 46, 171 (1966).

(2) B. Conforto, G. Fidecaro, H. Steiner, R. Bizzarri, P. Guidoni, F. Marcelja, G. Brautti, E. Castelli, M. Ceschia and M. Sessa: Nuovo Cimento 54 A, 441 (1968).

(3) R. Bizzarri, B. Conforto, G.C. Gialanella, P. Guidoni, F. Marcelja, E. Castelli, M. Ceschia and M. Sessa: Nuovo Cimento 54 A, 456 (1968).

(4) J.S. Ball and J.F. Chew: Phys.Rev. 109, 1385 (1958).

(5) For a comparison of these calculations with experimental data, see ref.(1) and(2).

(6) R.A. Bryan and R.J.N. Phillips, Nucl. Phys. B5, 201 (1968);
R.J.N. Phillips, Rev. Mod. Phys. 39, 681 (1967).

(7) R.A. Bryan and B.L. Scott: Phys.Rev. 135, B434 (1964).

(8) For recent reviews of the experimental situation for the S-meson see M. Laloum in Simposium on Nucleon-Antinucleon Annihilations, Chexbres 27-29 March 1972, CERN report 72-10 and E. Castelli: Boson resonances with mass close to the two nucleon mass: the S-region - presented at the Third Triangle Seminar, Trieste, May 1973. University of Trieste internal report INFN/AE-73/6.
The possibility of the S meson detection in the nucleon-antinucleon interaction is discussed by R. Bizzarri: Experimental survey of low energy antiproton -nucleon interaction - presented at the Seminar on "Interaction of High Energy Particles with Nuclei and New Nuclear - like Systems", Moscow, ITEP, September 1973. University of Rome internal report n. 508.

(9) R. Bizzarri, P. Guidoni, F. Marzano, E. Castelli, P. Poropat and M. Sessa, Phys. Rev. D6, 160 (1972).

(10) R.D. Burrows, D.E. Caro, E. Gold, A.G. Klein, C.E. MacDowell, J.L. Olney, G.I. Opat, J. Starr, J.W.G. Wignall and D.C. Peaslee: Aust. J. Phys. 23, 819 (1970).

(11) T. Hamada and J.D. Johnston: Nucl. Phys. 34, 382 (1962).

(12) W. Chinowsky and G. Kojoian: Nuovo Cimento 43 A, 684 (1966).

(13) V. Barnes, K.W. Lai, P. Anninos, L. Gray, P. Haggerty, E. Harth, T. Kalogeropoulos, S. Zenone, R. Bizzarri, U. Dore, G. Gialanella, G. Moneti and P. Guidoni, XII International Conference on High Energy Physics, Dubna 1964, pag. 731.

([14]) L. Gray, P. Haggerty and T. Kalogeropoulos: Phys. Rev. Lett. 26, 1491 (1971).

([15]) A. Bettini, M. Cresti, S. Limentani, L. Peruzzo, R. Santangelo, S. Sartori, L. Bertanza, A. Bigi, R. Carrara, R. Casali and P. Lariccia: Nuovo Cimento 47, 642 (1967).

([16]) P.S. Eastman, Z. Ming Ma, B.Y. Oh, D.L. Parker, G.A. Smith and R.J. Sprafka: Nucl. Phys. B51, 29 (1973).

([17]) B.Y. Oh, P.S. Eastman, Z. Ming Ma, D.L. Parker, G.A. Smith, R.J. Sprafka: Nucl. Phys. B 51, 57 (1973).

([18]) G. Ciapetti, R. Bizzarri, U. Dore, G.C. Gialanella, G.C. Moneti, P. Guidoni, P. Anninos, L. Gray, P. Haggerty, E. Harth, T. Kalogeropoulos and S. Zenone. Supplemento Nuovo Cimento 3, 1208 (1965).

([19]) I. Laakso, Ann. Acad. Sci. Fenn. Ser. A6, No. 292 (1968).

([20]) CERN - Collège de France Collaboration - unpublished results.

([21]) G. Alberi, E. Castelli, P. Poropat and M. Sessa: University of Trieste internal report I.N.F.N./A.E. - 72/3 (1972).

([22]) V. Franco and R.J. Glauber: Phys. Rev. 142, 1195 (1966).

FIGURE CAPTIONS

Fig. 1 - Orthogonal projection of the entrance and exit fiducial planes for the I and II - III exposures. The mean trajectories of the beam are drawn for all the four exposures; at the entrance fiducial plane the average momenta are respectively: 0) 340 MeV/c, I) 459 MeV/c, II) 540 MeV/c, III) 601 MeV/c. The mechanical support of the copper moderator is shown at left of the chamber together with the AA plane (see text).

Fig. 2 - Momentum distribution at the entrance fiducial region of 1421 non interacting tracks of exposure II as obtained from radius of curvature measurements.

Fig. 3 - Track length distribution of 4122 annihilating antiprotons in the 0 exposure.

Fig. 4 - Total (σ_t), inelastic (σ_i) and scattering (σ_s) cross-sections vs. laboratory kinetic energy and momentum. ◇ R.D. Burrows et al.([10]), • this work. Energy resolution curves for this experiment are shown on the abscissa axis. The results of the theoretical fit of ref.([6]) on $\bar{p}p$ cross-sections, multiplied by 2 are shown for reference.

Fig. 5 - a) momentum spectrum of protons from $\bar{p}d$ annihilations (1698 events above 120 MeV/c). The curve is the expected distribution from the Hamada-Johston ([11]) wave function normalized to the events (3407) below 120 MeV/c.
b,c) Distribution of the momentum components transverse (P_t) and parallel (P_ℓ) to the beam direction for the same protons. The curves refer to the Hamada-Johnston ([11]) predictions with a cut at 120 MeV/c.

Fig. 6 - Charged-prong annihilation ($\sigma_{i,2+4+6}$) and zero-prong ($\sigma_{i,o}$) cross-sections vs. laboratory kinetic energy and momentum in hydrogen (o U. Amaldi et al. ([1])) and in deuterium (◇ R.D. Burrows et al.([10]), • this work).

Fig. 7 - Inelastic cross-sections vs. laboratory kinetic energy and momentum in hydrogen ($\sigma_{i,p}$ - o U. Amaldi et al.([1])) and in deuterium ($\sigma_{i,p}$ and $\sigma_{i,n}$ - • this work). The curves are theoretical calculations by R.A. Bryan and R.J.N. Phillips ([6]).

Fig. 8 - Distribution in the laboratory frame of the cosine of the fitted angle between the beam and positive track for the 1743 scattering events of II exposure in which this positive track is visible.

Fig. 9 - Differential cross-sections $d\sigma/d|t|$ for $|t| \leq 0.08$ $(GeV/c)^2$ at the nine incident energies. At t=0 the optical point is indicated. The first point plotted at each energy is measured on a bin size variable with energy according to the minimum detectable scattering angle. The limits of this first bin are given below together with the number of events at each energy. For lower values the interval size is given:
a) 57.4 MeV; 654 events; 0.0020 - 0.0025.
b) 79.8 MeV; 952 events; 0.0020 - 0.0025.
c) 98.1 MeV; 996 events; 0.0030 - 0.0050.
d) 109.3 MeV; 988 events; 0.0030 - 0.0050.
e) 124.1 MeV; 1192 events; 0.0040 - 0.0050.
f) 137.7 MeV; 1353 events; 0.0040 - 0.0050.
g) 146.6 MeV; 1360 events.
h) 158.8 MeV; 1668 events.
i) 170.5 MeV; 1641 events.

TABLE I

Exposure	0	1	2	3
Entrance momentum (MeV/c)	340	459	540	601
Exit momentum (MeV/c)		287	448	532
Length of track in fiducial volume (Km)		6.94	10.77	15.00
Accepted interactions	4122	9322	12149	16101
% rejected	67	44	34	25

TABLE II

Laboratory kinetic energy $T_{\bar{p}}$ (MeV)	Laboratory incident momentum $P_{\bar{p}}$ (MeV/c)	Cross-sections (mb)							
		$\sigma_{i,o}$	$\sigma_{i,2+4+6}$	$\sigma_{i,p}=\sigma_{i,o}+\sigma_{i,2+4+6}$	$\sigma_{i,n}=\sigma_{a,n}$	$\sigma_i=\sigma_{i,p}+\sigma_{i,n}$	σ_s	$\sigma_t=\sigma_s+\sigma_i$	$\sigma_{i,n}$ (proton spectator not visible)
57.4 13.2	333. 40.	15.0 1.5	115.8 5.7	130.8 6.1	110.0 5.3	240.8 8.3	125.4 5.2	366.2 11.5	64.7 3.4
79.8 10.0	395. 26.	15.0 1.3	111.9 4.6	126.9 4.9	94.4 4.1	221.3 6.2	125.1 4.3	346.4 8.4	53.8 2.6
98.1 8.5	440. 20.	11.6 1.0	111.9 4.1	123.5 4.3	85.9 3.5	209.4 5.3	121.9 3.8	331.3 7.1	50.3 2.3
109.3 8.8	466. 20.	13.7 1.1	100.0 3.9	113.7 4.2	84.9 3.5	198.6 5.4	112.1 3.7	310.7 7.3	49.9 2.3
124.1 8.1	498. 17.	12.4 .9	87.4 3.2	99.8 3.5	75.5 2.9	175.3 4.4	112.2 3.3	287.5 6.1	44.2 1.9
137.7 7.5	527. 16.	11.6 .8	85.5 2.9	97.1 3.1	75.7 2.7	172.8 3.9	110.6 3.0	283.4 5.4	43.3 1.7
146.6 7.1	545. 14.	12.1 .9	85.9 3.0	98.0 3.2	76.9 2.8	174.9 4.0	107.7 3.0	282.6 5.4	43.1 1.7
158:8 6.7	569. 13.	13.2 .8	81.1 2.6	94.3 2.8	74.5 2.5	168.8 3.5	114.1 2.7	282.9 4.8	42.8 1.6
170.5 6.4	591. 12.	11.2 .7	83.5 2.5	94.7 2.6	68.1 2.2	162.8 3.1	109.0 2.5	271.8 4.2	37.8 1.4
0	0	0.029 0.003	0.522 0.015	0.551 0.015	0.449 0.014	1.0	-	-	0.272 0.008

TABLE III

Laboratory kinetic energy $T_{\bar{p}}$ (MeV)	Laboratory incident momentum $P_{\bar{p}}$ (MeV/c)	Cross-sections (mb)						$R' = \frac{\sigma_{i,n}}{\sigma_{i,p}}$	$R'' = \frac{\sigma_{i,n}}{\sigma_{i,2+4+6}}$	$R = \frac{\sigma_{a,n}}{\sigma_{a,p}}$
		σ_1	σ_2	σ_3	σ_4	σ_5	σ_6			
57.4 13.2	333. 40.	16.0 1.7	53.2 3.1	70.6 3.9	56.9 3.7	23.3 2.1	5.6 1.2	.841 .056	.950 .065	.882 .058
79.8 10.0	395. 26.	16.0 1.5	47.9 2.5	56.9 3.0	57.6 3.1	21.5 1.7	6.4 1.1	.744 .042	.844 .049	.781 .045
98.1 8.5	440. 20.	14.2 1.3	46.3 2.3	48.3 2.5	59.8 2.8	22.6 1.6	5.8 1.0	.696 .037	.768 .041	.730 .039
109.3 8.8	466. 20.	11.9 1.1	46.5 2.2	52.9 2.6	49.2 2.6	19.2 1.5	4.1 .8	.747 .040	.849 .047	.783 .042
124.1 8.1	498. 17.	11.4 1.0	38.3 1.8	45.3 2.1	44.4 2.2	18.6 1.3	3.8 .8	.756 .039	.864 .045	.794 .040
137.7 7.5	527. 16.	9.8 .9	35.5 1.6	46.3 2.0	44.2 2.0	19.1 1.2	5.5 .8	.780 .037	.885 .042	.818 .037
146.6 7.1	545. 14.	11.3 .9	39.1 1.7	48.0 2.1	41.6 2.0	17.6 1.2	5.2 .8	.785 .038	.895 .045	.823 .039
158.8 6.7	569. 13.	12.0 .9	33.6 1.4	43.5 1.8	43.5 1.8	18.6 1.1	3.6 .6	.790 .034	.919 .042	.829 .037
170.5 6.4	591. 12.	8.7 .7	33.7 1.3	42.7 1.7	44.1 1.7	16.1 1.0	5.3 .7	.719 .030	.816 .035	.755 .031
0	0	0.068 0.005	0.239 0.008	0.260 0.010	0.261 0.010	0.119 0.007	0.022 0.004	-	-	0.815 0.034

TABLE IV

Annihilation channel	Charge of π	$\langle n \rangle$ in $\bar{p}N$	$\langle n \rangle$ in $\bar{p}d$
$\bar{p}p$	+	1.6	0.9
$\bar{p}p$	o	1.9	1.1
$\bar{p}n$	o	2.0	0.9
$\bar{p}n$	-	2.1	0.9

T A B L E V

$\frac{d\sigma}{dt} \pm \Delta \frac{d\sigma}{dt}$ mb/(GeV/c)²

$-t$ (GeV/c)² \ $T_{\bar{p}}$ MeV	57.4		79.8		98.1		109.3		124.1		137.7		146.6		158.8		170.5	
optical point	6838	429	6020	294	5583	239	4925	231	4217	178	4083	155	3980	153	4068	138	3746	116
0.0000-.0025	5883	1470*	5483	1197*														
.0025-.0050	6628	704	3831	446	4322	501*	3671	439*	3930	576*	2351	416*						
.0050-.0075	4569	574	3368	414	3499	400	3340	372	3212	329	2795	286	2723	273	2589	246	2513	235
.0075-.0100	4072	536	3377	412	3351	388	2856	341	2844	307	3018	296	2788	274	2902	259	2841	248
.0100-.0125	3392	484	4148	455	2789	352	2701	330	2717	298	2421	264	2685	268	2741	251	2017	208
.0125-.0150	2961	450	3147	393	2408	325	2562	319	2153	264	1803	226	2164	239	2153	221	1893	201
.0150-.0175	3189	465	2344	336	2120	303	2107	288	1969	251	2044	240	1656	208	2064	216	2133	212
.0175-.0200	2183	381	2276	330	2321	316	1508	242	1762	236	1779	223	1388	189	1606	189	1658	186
.0200-.0225	1634	329	2106	315	2084	298	1684	255	1346	206	1790	222	1841	218	1660	192	1606	183
.0225-.0250	1176	279	1954	303	1649	265	1185	213	1492	216	1234	184	1323	184	1561	185	1284	163
.0250-.0275	1372	301	1477	262	1513	252	1134	208	1142	188	1252	185	1390	188	1488	181	1379	168
.0275-.0300	1634	328	1468	261	1542	254	1501	238	1041	179	1137	175	978	156	1043	151	1332	165
.0300-.0325	2026	366	1697	280	1575	255	1196	211	1343	203	1130	174	1299	180	1084	153	1059	146
.0325-.0350	1438	307	1147	230	1160	219	1226	214	1124	185	1280	185	966	155	1248	164	1119	151
.0350-.0375	915	245	1238	239	1234	225	737	165	1237	193	1065	168	1009	158	987	145	706	119
.0375-.0400	980	253	1151	231	861	188	991	191	869	161	1034	165	786	139	983	145	626	112
.0400-.0425	588	196	1238	239	1271	228	844	176	717	147	714	137	613	122	871	136	700	118
.0425-.0450	653	207	1055	220	902	192	844	176	596	133	893	153	752	135	676	119	657	114
.0450-.0475	196	113	550	159	824	184	778	169	744	148	761	141	750	135	801	130	673	115
.0475-.0500	457	173	917	205	779	179	917	184	741	148	732	138	652	125	879	135	673	115
.0500-.0525	392	160	780	189	615	159	624	151	536	126	683	134	362	93	776	127	671	115
.0525-.0550	522	185	458	145	410	129	550	142	622	136	649	130	455	104	542	106	587	107
.0550-.0575	261	130	458	145	410	129	367	116	385	107	415	104	556	116	418	93	527	101
.0575-.0600	65	65	412	137	533	148	256	97	682	142	467	110	335	89	310	80	448	93
.0600-.0625	196	113	412	137	410	129	256	97	385	107	467	110	407	98	351	85	329	80
.0625-.0650	261	130	275	112	615	159	367	116	444	115	389	100	311	86	372	87	389	87
.0650-.0675	65	65	321	121	410	129	183	82	444	115	337	93	335	89	517	103	290	75
.0675-.0700	130	92	321	121	205	91	550	142	533	126	493	113	311	86	289	77	271	72
.0700-.0725	65	65	137	79	410	129	403	121	266	89	207	73	215	71	207	65	252	69
.0725-.0750	196	113	229	102	205	91	256	97	237	83	389	100	215	71	144	54	368	84
.0750-.0775	130	92	183	91	123	71	146	73	207	78	207	73	215	72	207	65	193	61
.0775-.0800	65	65	91	64	123	71	146	73	355	102	259	82	191	67	310	80	213	64
.0800-.0900	81	36	114	36	133	36	146	36	177	36	272	42	203	34	258	36	179	29
.0900-.1000	0		68	28	153	39	119	33	133	31	136	29	167	31	186	31	135	25
.1000-.1100	0		57	25	61	25	91	29	74	23	129	29	83	22	119	24	116	23
.1100-.1200	16	16	22	16	83	29	45	20	103	27	103	25	83	22	119	24	87	20
.1200-.1300	17	18	11	11	51	22	36	18	22	12	64	20	71	20	108	23	78	19
.1300-.1400	16	16	34	19	11	11	36	18	29	14	45	17	41	15	46	15	92	21
.1400-.1500	0		11	11	20	14	27	15	51	19	51	18	42	15	41	14	24	10
.1500-.1600	32	23	47	23	20	14	36	18	14	10	38	15	11	8	25	11	38	13
.1600-.1700	0		34	19	41	20	9	9	22	12	25	13	11	8	36	13	14	8
.1700-.1800	16	16	0		0		18	12	29	14	19	11	11	8	20	10	24	10
.1800-.1900	0		22	16	0		27	15	22	12	27	13	29	13	10	7	19	9
.1900-.2000	0		11	11	10	10	27	15	51	19	25	12	5	5	25	11	9	6
.2000-.2100	0		0		20	14	9	9	7	7	12	9	0		15	8	9	6
.2100-.2200	0		0		0		0		22	12	12	9	11	8	10	7	29	11
.2200-.2300	0		0		20	14	0		22	12	12	9	12	8	15	8	0	
.2300-.2400	0		0		0		9	9	0		6	6	5	5	15	8	4	4
.2400-.2500	0		0		30	17	9	9	0		0		11	8	5	5	19	9
.2500-.2600	0		0		0		9	9	14	10	0		0		5	5	24	10
.2600-.2700	0		0		20	14	9	9	0		6	6	17	10	25	11	9	6
.2700-.2800	0		0		10	10	0		22	12	0		5	5	15	8	9	6
.2800-.2900	0		0		10	10	0		0		0		5	5	5	5	14	8
.2900-.3000	0		0		0		0		0		0		0		15	8	4	4

* see caption of Fig. 9

T A B L E VI

$T_{\bar{p}}$(MeV)	ƛ(fm) *	b(fm²)	R = $2\sqrt{b}$ (fm)
57.4	1.20	2.50 ± 0.20	3.16 ± 0.13
79.8	1.02	1.93 ± 0.17	2.78 ± 0.12
98.1	0.92	2.04 ± 0.17	2.86 ± 0.12
109.3	0.87	2.17 ± 0.17	2.95 ± 0.12
124.1	0.82	1.84 ± 0.15	2.71 ± 0.11
137.7	0.78	1.79 ± 0.14	2.68 ± 0.10
146.6	0.75	1.80 ± 0.14	2.68 ± 0.10
158.8	0.72	1.67 ± 0.12	2.58 ± 0.09
170.5	0.70	1.67 ± 0.12	2.58 ± 0.09

* ƛ is the relative $\bar{p}$-nucleon at rest wavelength.

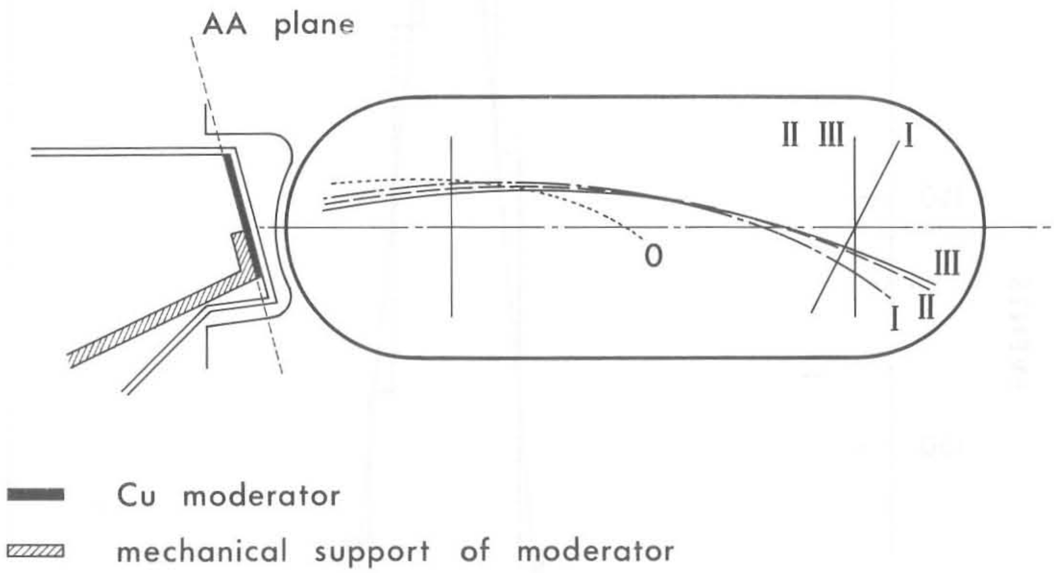
AA plane
II III
I
0
III
I II
Cu moderator
mechanical support of moderator

Fig. 1

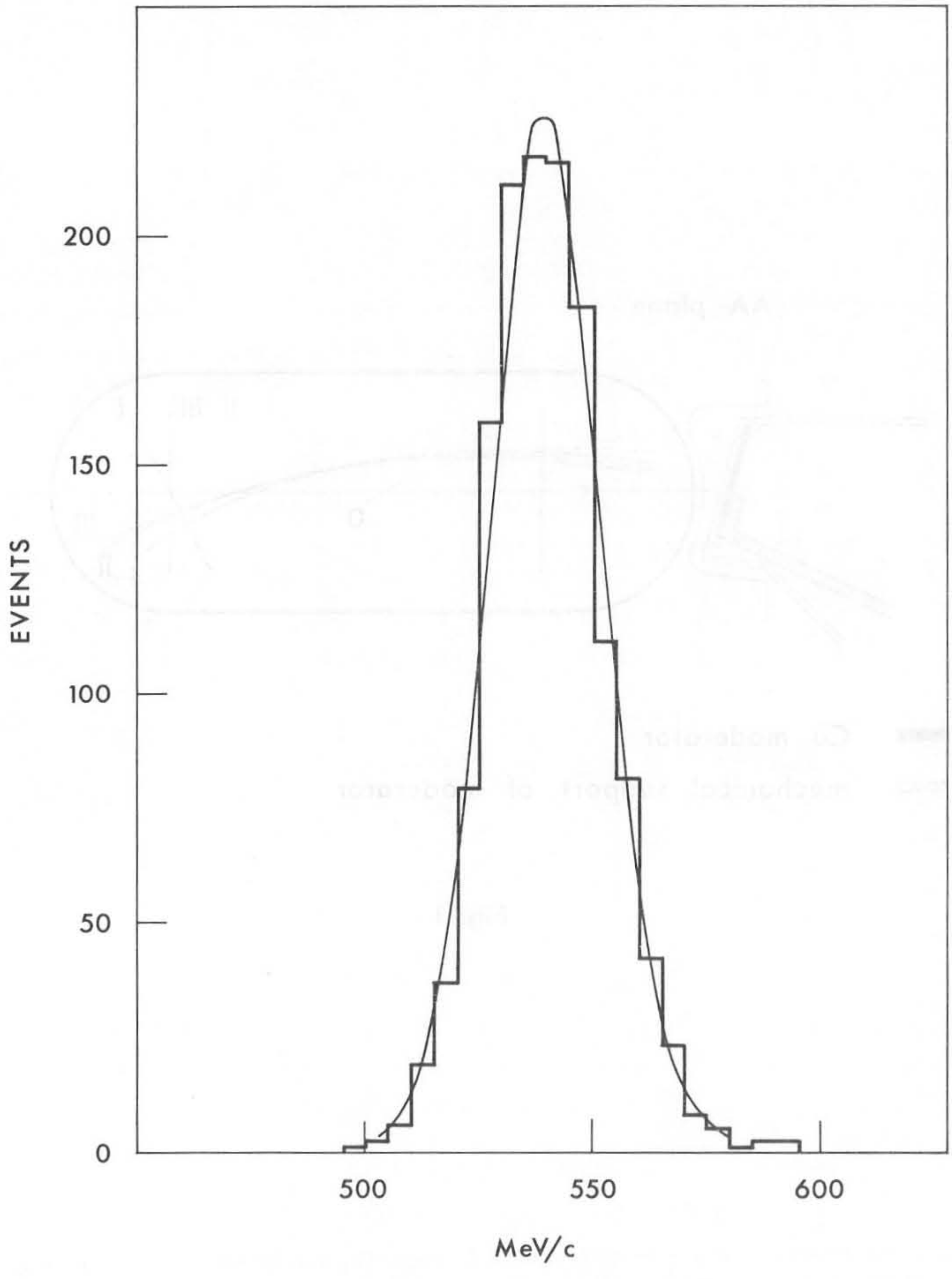

Fig. 2

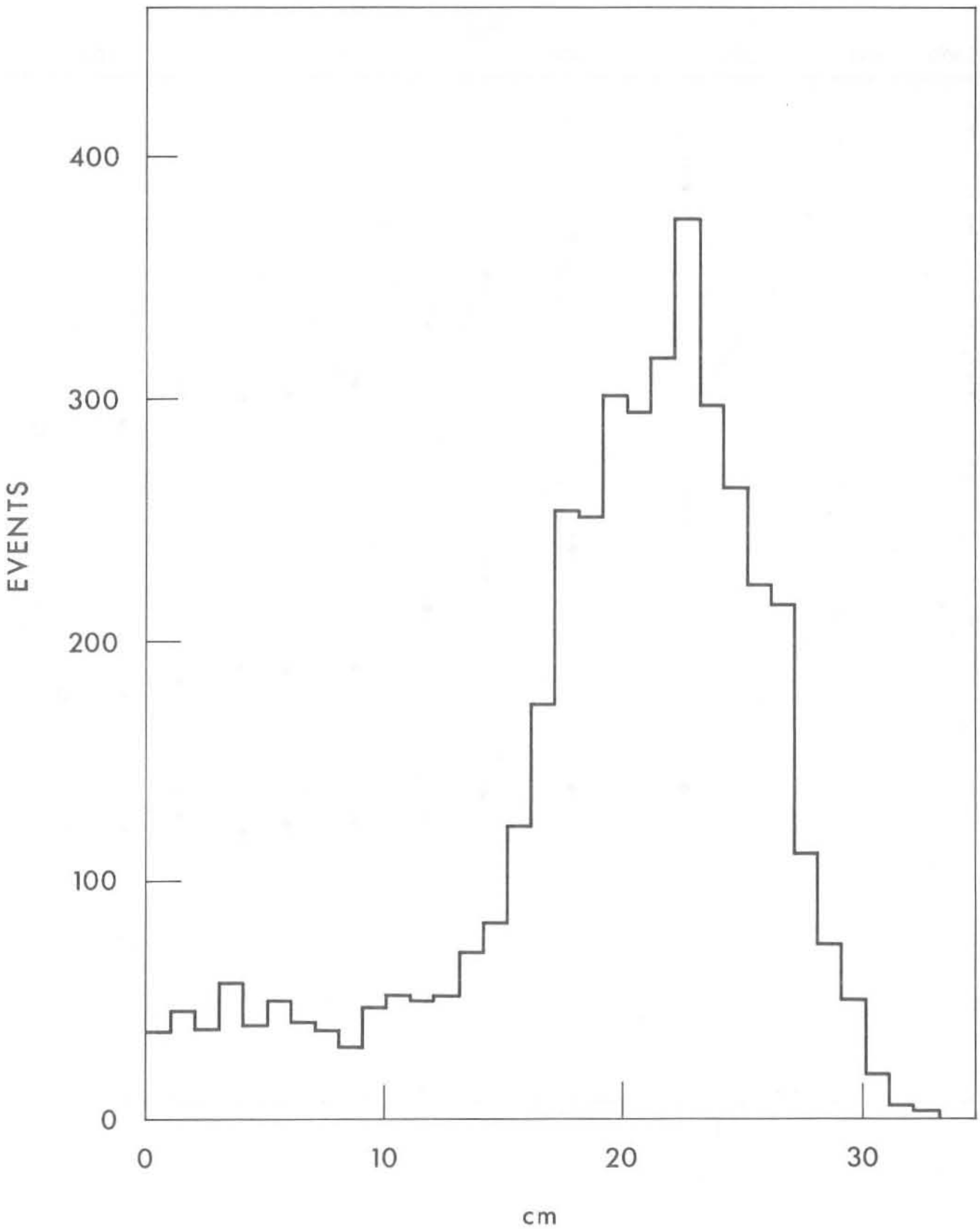

Fig. 3

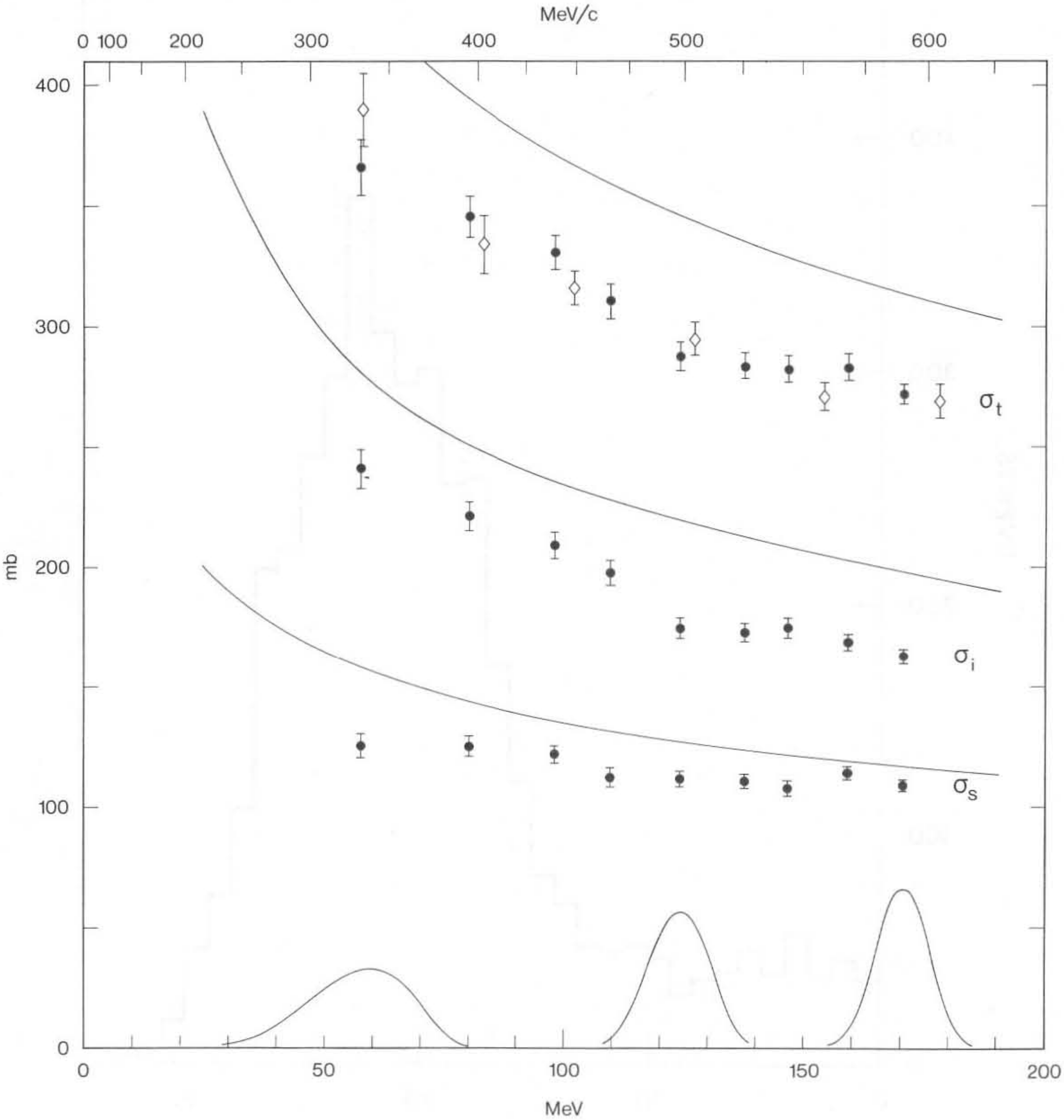

MeV/c
0 100
200
300
400
500
600
400
300
200
100
0
mb
σt
σi
σs
0
50
100
150
200
MeV

Fig. 4

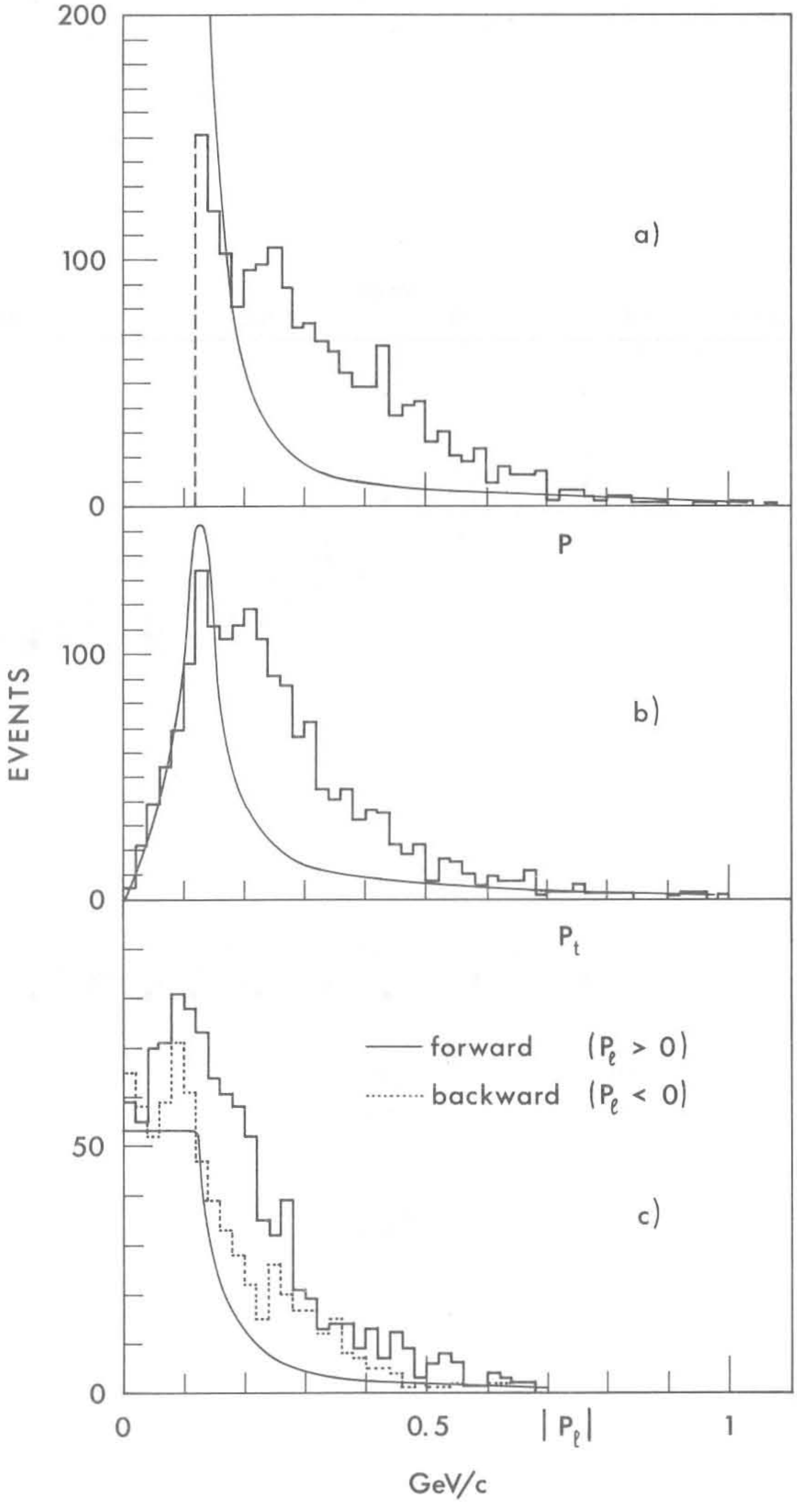
200
100
0
a)
P
100
0
b)
EVENTS
P_t
forward (P_ℓ > 0)
backward (P_ℓ < 0)
50
0
c)
0
0.5
|P_ℓ|
1
GeV/c

Fig. 5

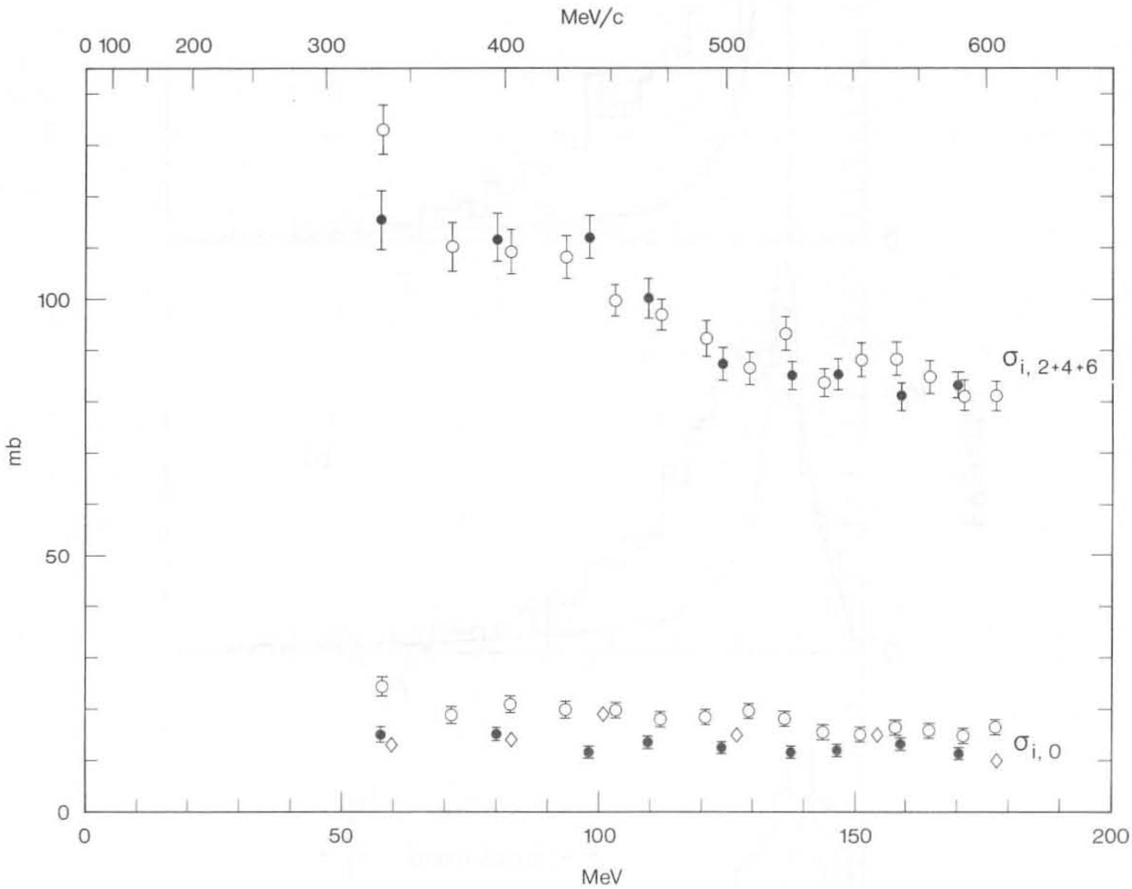
MeV/c
0 100
200
300
400
500
600
mb
100
50
0
0
50
100
150
200
MeV
σi, 2+4+6
σi, 0

Fig. 6

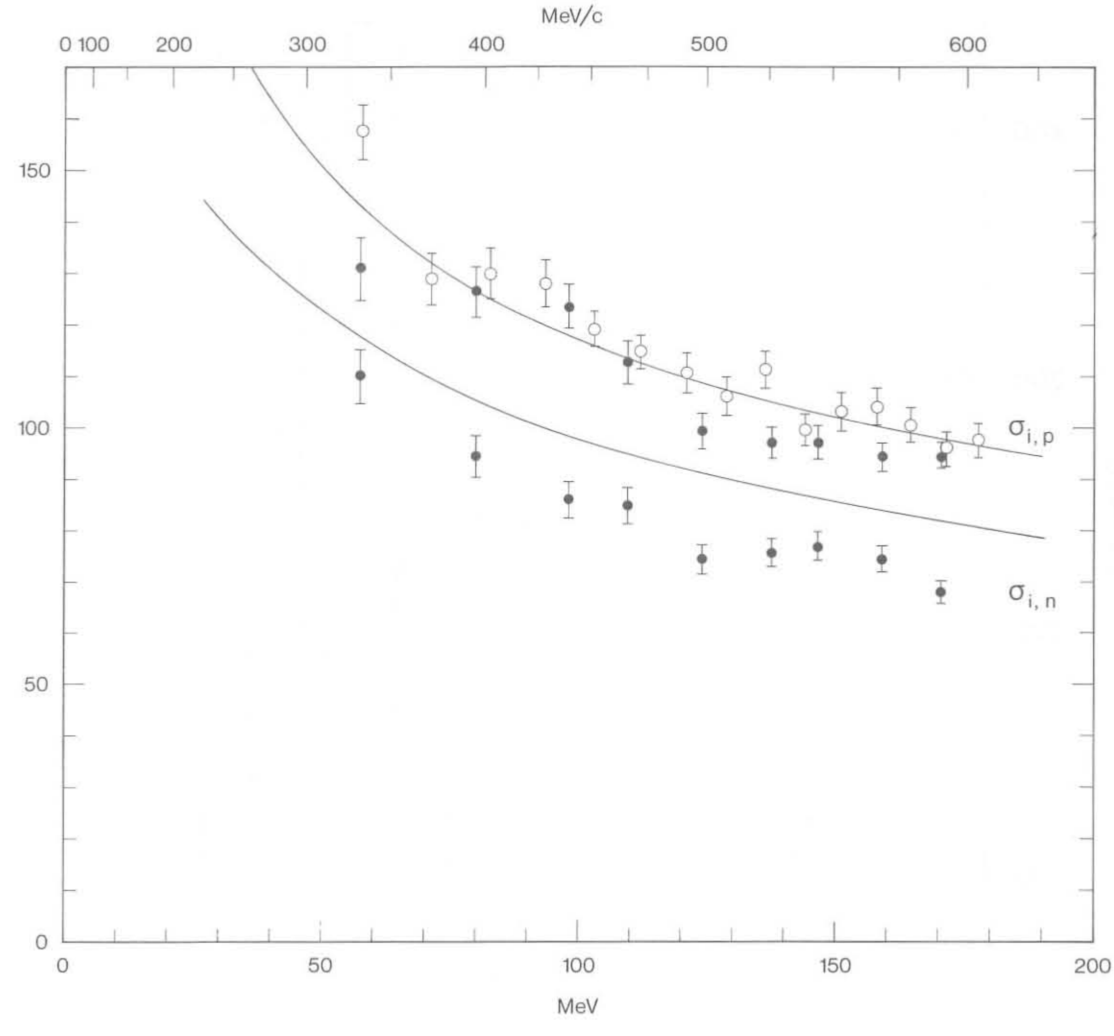

MeV/c
0 100
200
300
400
500
600
150
100
50
0
0
50
100
150
200
MeV
$\sigma_{i,p}$
$\sigma_{i,n}$

Fig. 7

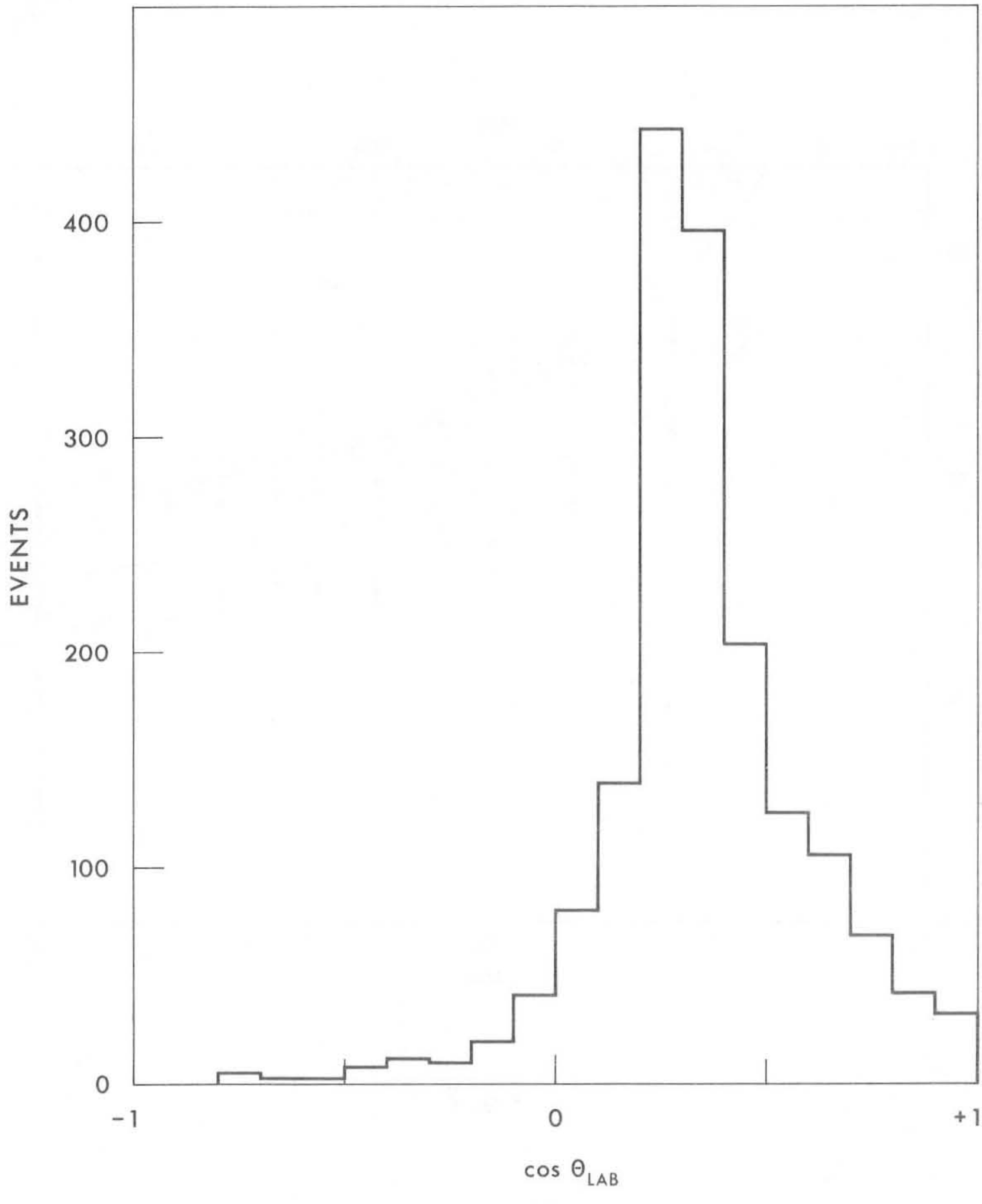

Fig. 8

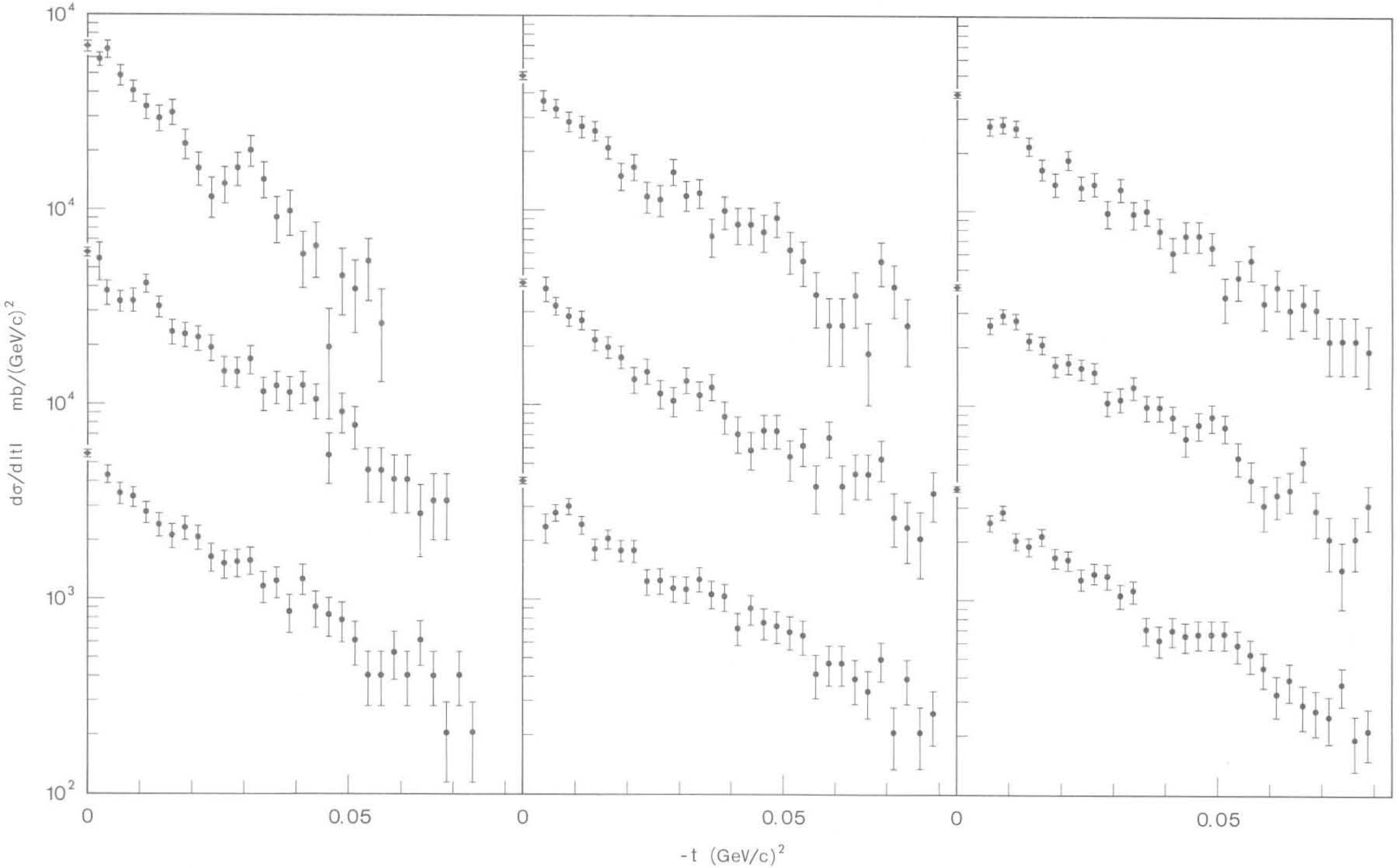

Fig. 9